

# Structural analysis of as-deposited and annealed low-temperature gallium arsenide

R.J. Matyi <sup>a</sup>, M.R. Melloch <sup>b</sup> and J.M. Woodall <sup>c</sup>

<sup>a</sup> *Department of Materials Science and Engineering, University of Wisconsin, Madison, Wisconsin 53706, USA*

<sup>b</sup> *School of Electrical Engineering, Purdue University, West Lafayette, Indiana 47907, USA*

<sup>c</sup> *IBM Research Division, Thomas J. Watson Research Center, Yorktown Heights, New York 10598, USA*

Received 16 September 1992; manuscript received in final form 15 December 1992

The structure of GaAs grown at low substrate temperatures (LT-GaAs) by molecular beam epitaxy has been studied using high resolution X-ray diffraction methods. Double crystal rocking curves from the as-deposited LT-GaAs show well defined interference fringes, indicating a high level of structural perfection. Triple crystal diffraction analysis of the as-deposited sample showed significantly less diffuse scattering near the LT-GaAs 004 reciprocal lattice point compared with the substrate 004 reciprocal lattice point, suggesting that despite the incorporation of approximately 1% excess arsenic, the epitaxial layer had superior crystalline perfection than did the GaAs substrate. Triple crystal scans of annealed LT-GaAs showed an increase in the integrated diffuse intensity by approximately a factor of three as the anneal temperature was increased from 700 to 900°C. Analogous to the effects of SiO<sub>2</sub> precipitates in annealed Czochralski silicon, the diffuse intensity is attributed to distortions in the epitaxial LT-GaAs lattice by arsenic precipitates.

## 1. Introduction

Gallium arsenide epitaxial layers grown at low substrate temperatures (LT-GaAs) have attracted considerable attention recently due to both their interesting structural and electrical properties, and their potential usefulness in advanced device applications. Following growth by molecular beam epitaxy (MBE) at temperatures in the vicinity of 200°C, LT-GaAs films that are annealed at elevated temperatures exhibit extremely high resistivities and breakdown strengths. Significant improvements in the performance of GaAs devices fabricated using LT-GaAs buffer layers have been reported [1,2].

Because of the potential of this material for device applications and the unusual MBE growth conditions, numerous studies have been performed recently to elucidate the microstructural properties of LT-GaAs [3]. Transmission electron microscopy (TEM) analyses of as-grown LT-GaAs have shown no evidence of structural defects in

layers grown at 200°C, even though X-ray diffraction, electron paramagnetic resonance, and analytical TEM measurements indicated a high level (approximately 1%) excess arsenic [4–7]. Following post-growth annealing at 600°C, TEM examinations have shown that the excess arsenic forms arsenic precipitates that are generally uniformly dispersed throughout the epitaxial layer [7–9]. High resolution TEM analyses have shown that the smaller As precipitates (2 to 3 nm in diameter) are coherent with the GaAs lattice, while larger precipitates lose their coherency [10].

X-ray diffraction has been used extensively for characterizing LT-GaAs and for observing the effects of postgrowth annealing on the structure and perfection of this material. X-ray rocking curves of as-grown LT-GaAs typically show that the lattice parameter is larger than that of bulk GaAs [4,7], although recent work by Fatemi and coworkers showed large variations in the separation of the substrate and LT-GaAs diffraction peaks with little correlation between growth tem-

perature and peak separation [11]. Wie and coworkers reported that the lattice parameter of LT-GaAs changed abruptly at an anneal temperature of around 350°C, where the perpendicular lattice mismatch decreases significantly [12,13]. Annealing at higher temperatures results in complex behavior; various X-ray studies have reported the lattice parameter of annealed LT-GaAs to can be greater than, less than, or equal to that of the GaAs substrate [4,5,11–13].

As mentioned above, one effect of post-growth annealing in LT-GaAs is to produce As-rich precipitates. The development of second-phase precipitates within the GaAs epitaxial single crystal matrix would be expected to generate strains in the GaAs lattice due to the change in volume associated with the precipitation process. Precipitation-induced strains are well known in the formation of oxygen precipitates in Czochralski silicon following a high-temperature anneal where the interstitial oxygen (typically present at supersaturations of several parts per million) forms thermodynamically-stable SiO<sub>2</sub> precipitates. The change in volume that arises from the oxygen precipitates tends to “punch out” dislocation loops which are effective as internal gettering sites for metallic impurities in CZ-silicon [14].

Recently it has been shown that the use of high resolution diffraction techniques can reveal significant details concerning the crystallographic structure and properties of epitaxial layers [15]. Because of these unique capabilities, we have conducted a high resolution X-ray diffraction analysis of LT-GaAs grown by MBE to better understand the structure of the as-grown material and to clarify the effects of postgrowth processing on this material. Some preliminary results have been published elsewhere [16].

## 2. Experimental procedure

Details concerning the growth and characterization of the films studied in this work have been described earlier [16]. Briefly, all films used in this work were grown in a Varian GEN II MBE system on two-inch diameter undoped <001>

GaAs substrates. Layers with a thickness of approximately 1 μm were grown without intentional doping at a substrate temperature of 225°C on top of a 0.5 μm GaAs buffer layer grown at 600°C. Following growth, samples were annealed at 700, 800, and 900°C for a duration of 30 s in a computer-controlled mini-pulse rapid thermal processor. These anneals resulted in the formation of As precipitates from the excess As that was incorporated during the low temperature growth. Transmission electron microscopy showed that the average diameter of the precipitates increased while their density decreased with increasing anneal temperature [9].

High resolution X-ray diffraction analyses were performed using a Bede 150 double crystal diffractometer. Instead of the conventional single reflection monochromator, a pair of grooved silicon crystals was used in which the incident X-ray beam executed four (220) reflections in the (–, +, +, –) geometry [15,17]. Copper Kα<sub>1</sub> radiation was obtained from a Rigaku RU200 rotating anode generator. The two-crystal, four-reflection monochromator was physically integrated onto the Bede diffractometer in place of the conventional incident beam pinhole collimator. Since the monochromator conditioned the X-ray beam in an angular sense without limiting its spatial extent, a relatively large beam size on the sample (6 mm<sup>2</sup>) could be used.

The X-ray analysis of the LT-GaAs samples employed both double crystal and triple crystal diffraction scans. Double crystal rocking curves were recorded with the sample situated on the first axis of the diffractometer (i.e. in the location usually used for the monochromator in the double crystal geometry); the diffracted X-rays from the sample were recorded with a wide-open scintillation counter. Triple crystal scans were recorded by placing a triple bounce (220) grooved silicon crystal on the second axis and operating the instrument as a triple crystal diffractometer. By analyzing the angular distribution of the diffracted intensity from the sample, it was possible to separate the relatively weak scattering due to structural defects in the epitaxial layer from the much stronger diffracted intensity from the relatively perfect substrate [17].

### 3. Results

Fig. 1 illustrates a (004) double crystal rocking curve recorded using a  $1''$  angular step size from the as-grown unannealed LT-GaAs sample. Also shown in the figure is a simulated diffraction profile that was calculated using commercial rocking curve analysis software [18]. Comparison of the experimental and simulated rocking curves yielded a best visual fit when the perpendicular mismatch was assumed to be 0.133%. This value for a sample grown at  $225^\circ\text{C}$  is consistent with the results of Wie et al., who reported a perpendicular lattice mismatch in LT-GaAs of 0.15% and 0.10% for layers grown at  $200^\circ\text{C}$  and  $250^\circ\text{C}$ , respectively [13].

In performing the simulation shown in fig. 1, a number of important assumptions were made. First, the simulated rocking curve was calculated with the inclusion of sample curvature by convoluting the profile with a  $13''$  wide rectangle. The simulation also assumed perfect pseudomorphic strain in the LT-GaAs. Rocking curves recorded using an asymmetric (224) reflection showed a change in peak separation from  $174''$  to  $31''$ ; this

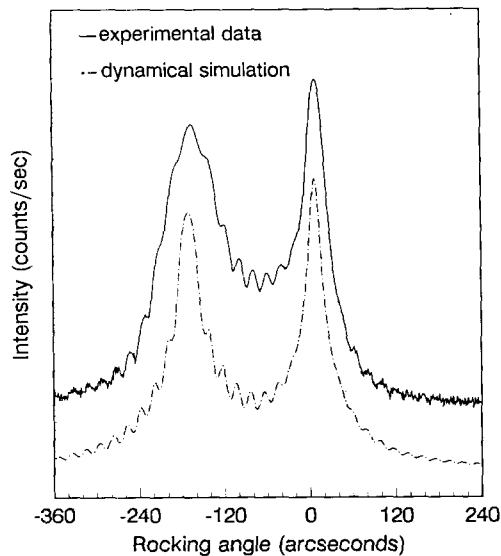


Fig. 1. Experimental and calculated (004) double crystal rocking curves for as-grown LT-GaAs sample (the rocking curves have been offset vertically for clarity): (a) experimental profile; (b) rocking curve calculated via dynamical simulation.

change agreed to within one arcsecond with the peak separations anticipated for a tetragonally distorted, fully coherent layer. As discussed below, the presence of interference fringes also suggests perfect pseudomorphic growth.

The rocking curve simulation assumed that pure  $\sigma$ -polarized X-rays from a single reflection silicon (220) reference crystal were used. By neglecting the  $\pi$ -polarized component a lack of agreement in the calculated and observed intensities would be anticipated. However, since the  $\pi$ -polarization component is reduced by  $\cos 2\theta_B$  per reflection (or to about 8.5% of its initial intensity following four Si (220) reflections and a single (004) reflection from the sample [19]) the effect of assuming pure  $\sigma$ -polarization is expected to be small. The simulation also assumed uniform strains and the absence of composition gradients, and no effort was made to accurately model the effect of these nonuniformities on the either the width or intensity of the rocking curve. The combined effects of all of these assumptions would be to reduce the agreement between the observed and simulated diffraction scans. Nevertheless, the various simplifications would not be expected to significantly alter the positions of the various maxima in the rocking curves, the determination of which was the prime motivating factor for performing the simulation.

In addition to the substrate and epitaxial layer (004) reflections, the experimental rocking curve in figure 1 shows very well-defined interference fringes. These fringes arise from the interaction of the diffracted intensities from the substrate and the epitaxial layer; their angular separation  $\Delta\theta$  is given by

$$\Delta\theta = \lambda\gamma_h/t \sin 2\theta_B, \quad (1)$$

where  $t$  is the layer thickness,  $\lambda$  is the X-ray wavelength,  $\theta_B$  is the Bragg angle, and  $\gamma_h$  is the cosine of the angle between the inward surface normal and the diffracted beam wavevector [20]. An agreement between the positions of the simulated and experimental fringes of better than one arcsecond was achieved by assuming a layer thickness of  $9850 \text{ \AA}$  instead of the assumed  $1 \mu\text{m}$  from the nominal MBE growth conditions. Since

the visibility of the fringes requires high spatial coherence of the diffracted X-ray wavefields, their presence is evidence of a high degree of structural perfection in the epitaxial layer.

The clear visibility of the interference fringes is surprising, since the fact that the angular separation of the epitaxial layer and substrate peaks corresponds to an interstitial As concentration of greater than 1% [12,13]. Given this high level of interstitial atoms, one might suspect that a strong dynamical interaction between the diffracted beams from both the layer and substrate could not exist. Since the relative intensities of the maxima and minima of the interference fringes match so well the values predicted from the purely dynamical simulation, we must conclude that the interstitial arsenic is distributed very uniformly throughout the GaAs lattice. Any clustering of the arsenic into nuclei or “pre-precipitates” would lead to local distortions in the lattice that would reduce the magnitude of dynamical interactions; such behavior is well known in pre-precipitation behavior of Czochralski silicon [21].

Further information on the structure of the as-grown LT-GaAs can be obtained from triple crystal diffraction analyses. Fig. 2 shows triple crystal X-ray diffraction scans that were recorded from three samples: (a) a highly perfect germanium crystal with a nominal dislocation density of zero and without intentional doping; (b) a 1  $\mu\text{m}$  GaAs epitaxial layer grown under “normal” MBE conditions (1  $\mu\text{m}/\text{h}$  deposition rate, substrate temperature 600°C) on an exactly oriented  $\langle 001 \rangle$  GaAs substrate that was identical to those used for the LT-GaAs growth; and (c) the as-deposited LT-GaAs epitaxial layer. The triple crystal data were recorded by performing multiple scans of the sample crystal in 6" steps at a fixed analyzer crystal setting, with the analyzer incremented 12" between each scan. The angular deviations of the sample and analyzer crystals from the 004 reciprocal lattice point (RLP) were then converted into the orthogonal reciprocal space coordinates  $q_x$  and  $q_y$  using the relationships given by Iida and Kohra [22]. In contrast with the 1" angular step size used for the double crystal rocking curve

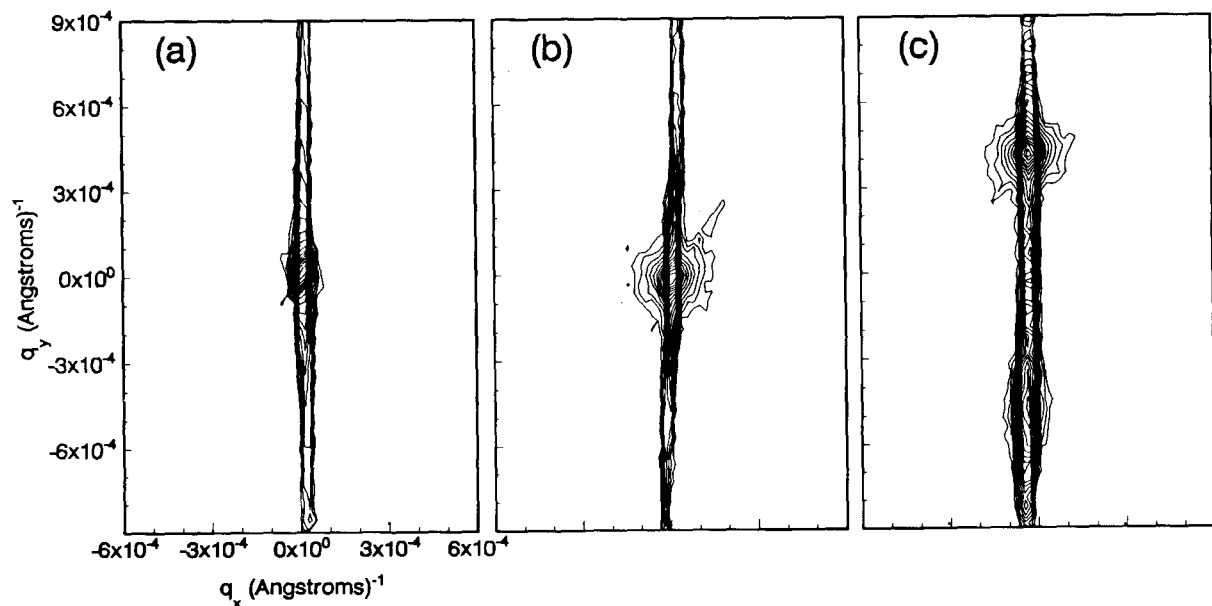


Fig. 2. (004) triple crystal scans from (a) highly perfect germanium; (b) GaAs with a 1  $\mu\text{m}$  GaAs layer grown at 600°C; (c) GaAs with a 1  $\mu\text{m}$  GaAs layer grown at 225°C. Scans (a) and (b) are centered on the 004 reciprocal lattice point for each substrate, while scan (c) is centered halfway between the 004 points of the substrate and the LT-GaAs layer. Identical ranges of  $q_x$  and  $q_y$  are used in all scans.

shown in fig. 1, the triple crystal angular step sizes (6" and 12") were too large to accurately record the narrow range of reflection of the GaAs (004) reflection; however, they were well suited for recording the diffuse intensity away from the main Bragg peak.

The intensities in fig. 2 are plotted as equal intensity contours on a logarithmic scale as a function of position in reciprocal space; the contours represent increments of 0.25 units of the logarithm of the measured intensity. The minimum contour level is  $10^{0.25}$  ( $\approx 1.8$ ) counts/s, which is much higher than the detection limit of about 0.5 counts/s (due to electronic noise and air scatter) for the diffraction system. Visible in the figure are the so-called "surface streaks" in the  $q_y$  direction which arises from the truncation of the crystal lattice at the sample surface [23]. The features that are visible in addition to the surface streak vary from sample to sample. In the case of the highly perfect germanium, for instance, very little additional scattering is present about the 004 RLP. This is consistent with a presumption of a high degree of structural perfection in this sample; it also demonstrates that excess scattering around a reciprocal lattice point cannot be attributed to instrumental effects. In contrast, the triple crystal scan from a GaAs epitaxial layer grown conventionally on a GaAs substrate shows a certain amount of diffuse scattering about the 004 point in reciprocal space. Although the origin of this scattering cannot be determined with certainty, we believe that it is due to dislocations and point defects in the GaAs substrate; similar triple crystal scans of GaAs wafers with no epitaxial layers have shown comparable patterns of diffracted intensity in reciprocal space [24]. There is a small amount of excess intensity oriented at an angle in reciprocal space with respect to the surface streak; this parasitic intensity arises from strong scattering from the sample crystal when it satisfies the Bragg condition irrespective of the analyzer crystal setting [17].

Comparison of fig. 2c with the scan from the highly perfect Ge (fig. 2a) and the GaAs control sample (fig. 2b) reveals several interesting features. First, the diffraction maxima from the epi-

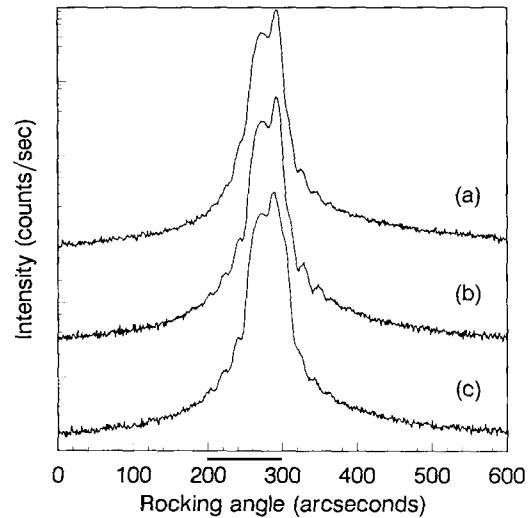


Fig. 3. (004) double crystal rocking curves from annealed LT-GaAs: (a) 700°C; (b) 800°C; (c) 900°C.

taxial layer (bottom) and the substrate (top) (004) reflections lie on the surface streak, as expected. The interference fringes that are clearly evident in the double crystal scan are also visible along the surface streak, although the relatively large step size used for the triple crystal scans reduces their visibility. There is a small amount of diffuse scattering about the 004 RLP corresponding to the substrate; comparison with fig. 2b indicates that this excess scattering is probably due to dislocations, residual surface polish damage, or other defects in the substrate. Examination of the 004 RLP corresponding to the epitaxial layer shows little if any diffuse scattering, thus suggesting again that the crystallographic quality of the LT-GaAs is exceedingly high, and may in fact be superior to that of the substrate.

Fig. 3 shows the (004) double crystal rocking curves recorded from the LT-GaAs samples following a 30 s anneal at 700, 800, and 900°C. While interference fringes are visible in all three rocking curves, they are much less pronounced than observed in the as-grown LT-GaAs. The sample annealed at 800°C appears to have the most distinct interference fringes, although the difference between the three samples is small. Analysis of these rocking curves showed that the difference in lattice parameter between the LT-

GaAs layer and the substrate decreases from 0.133% in the as-grown material to about 0.016% for each of the three anneal temperatures. As mentioned earlier, the work by Fatemi et al. [11] and Wie et al. [12,13] suggests that the LT-GaAs lattice parameter is highly sensitive to anneal conditions; we believe that the differences between our measurements and prior observations arise from the small differences in the annealing processes.

Fig. 4 illustrates the triple crystal diffraction scans from the annealed samples. Similar to the triple crystal scan from the as-deposited sample, the surface streak confirms the presence of interference fringes in the annealed samples, although again the large angular step size used in the triple crystal scans makes the fringes less evident. As reported earlier [16], a more important observation is the angular extent of the diffuse intensity perpendicular to the surface streak. The triple crystal scans show that the extent of this scattering is much larger than that seen in the as-deposited LT-GaAs and increases with increasing

anneal temperature. It should be noted that the reciprocal space scans shown in fig. 4 do not show the angled streaks of parasitic scattering seen in our earlier study [16]. Parasitic streaks due to strong scattering when the sample was on the exact Bragg condition have been removed by careful shielding of the analyzer crystal and detector during triple crystal data collection [17].

#### 4. Discussion

As mentioned previously, recent electron microscopy analyses of annealed LT-GaAs have shown that the average diameter of arsenic precipitates increases and their density decreases as the anneal temperature is increased [9]. Studies of oxygen precipitation in silicon have demonstrated that similar growth phenomena result in long-range distortions in the vicinity of precipitates, thus giving rise (for instance) to enhanced diffracted intensities under conditions such as those used for Lang scanning topography [25].

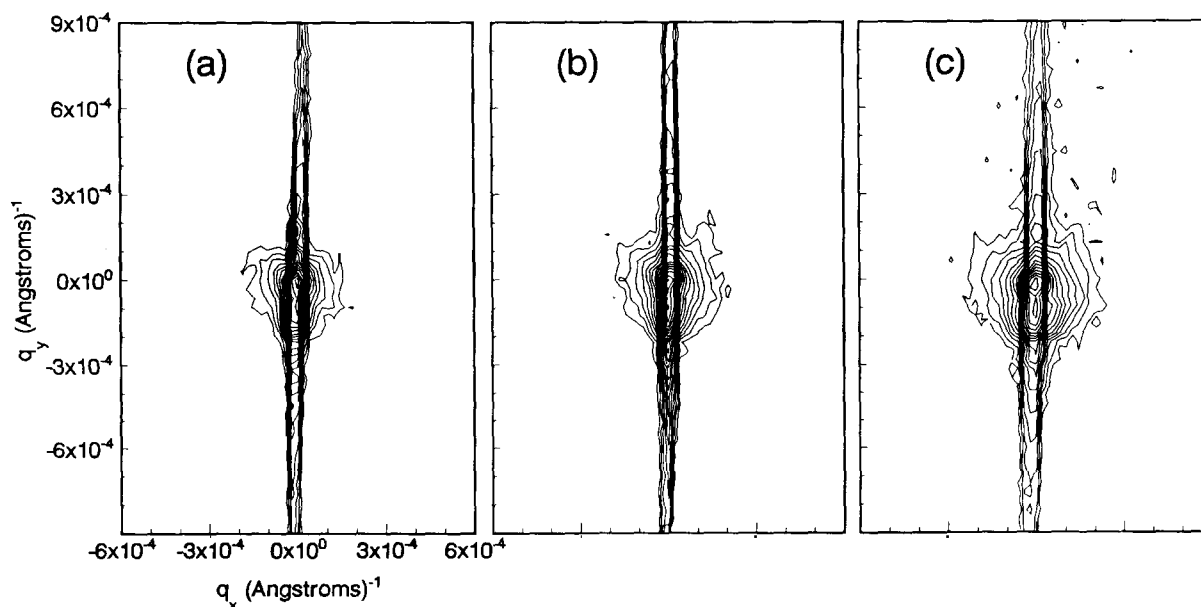


Fig. 4. (004) triple crystal scans from annealed LT-GaAs (identical ranges of  $q_x$  and  $q_y$  in all scans): (a) 700°C; (b) 800°C; (c) 900°C.

We believe that the increase in the extent of the X-ray scattering in the  $q_x$  direction is due to strain fields that arise from the arsenic precipitates in the annealed samples. These strain fields would locally increase the angular range over which Bragg diffraction could occur, thus increasing the angular extent of diffracted intensity observed in the  $q_x$  direction [15]. In other words, the “apparent mosaic spread” of the epitaxial layer increases with an increase in anneal time and average size of the arsenic precipitates. Dynamical diffraction effects would also be disrupted by the presence of precipitate strain fields; hence the reduction in the visibility of the interference fringes that was noted in the annealed samples would occur naturally during precipitate growth. Although the visibility of the interference fringes in the double crystal scans does not vary as strongly with anneal temperature as does the intensity distribution in the  $q_x$  direction, this difference may be due to the enhanced strain sensitivity of the triple crystal configuration.

The data in fig. 4 indicate an increase in the magnitude in diffuse scattering with increasing anneal temperatures; it would be desirable to be able to extract a single parameter from these scans to compare the effects of annealing on different samples. One method for doing this would be to integrate the diffuse intensity in reciprocal space and then use this integrated intensity as a measure of lattice distortion. A pleasing aspect of this approach is that the diffuse intensity is purely kinematic in nature and should thus be absent in ideally perfect crystals that diffract dynamically. This was evident in fig. 2a, where no diffuse scattering was observed in the triple crystal scan from a highly perfect germanium crystal. Hence we will define an “excess intensity”, which is the scattered intensity excluding the dynamical surface streak, as a measure of the kinematic scattering power and presumably an estimate of the level of structural imperfection in the sample.

In performing this integration it must be remembered that the total diffracted intensity should be present throughout a *volume* of reciprocal space. One can evaluate the excess intensity  $I_{\text{excess}}$  by performing a cylindrical integration of

the measured intensity according to the relation [24]

$$I_{\text{excess}} = 4\pi \int_{-q_y}^{+q_y} \int_{q_{x,\text{min}}}^{q_{x,\text{max}}} I_{\text{net}}(q_x, q_y) q_x dq_x dq_y. \quad (2)$$

In performing the integration, we will consider only the net intensity  $I_{\text{net}}(q_x, q_y)$  that is greater than some arbitrarily-assigned minimum level. In the case of the contour plots shown in figs. 2 and 4, for instance, an appropriate minimum level could correspond to the minimum contour level ( $10^{0.25} \approx 1.8$  counts/s) in the reciprocal space scans. We take the limits of integration for  $q$ , from the limits of the range of the reciprocal space scan in the  $q_y$  direction. For  $q_x$ , on the other hand, we choose as a lower limit some minimum value  $q_{x,\text{min}}$  such that the dynamical streak is not included in the integration, while the upper limit  $q_{x,\text{max}}$  corresponds to the limit of the reciprocal space scan in the  $q_x$  direction.

The net effect of these definitions for the integration limits and for  $I_{\text{net}}(q_x, q_y)$  is that a highly perfect sample such as the defect-free Ge shown in fig. 2 will exhibit  $I_{\text{excess}} = 0$ . Note that this represents one of the major advantages of triple crystal diffraction over the more common double crystal rocking curves, in that in the former method it is possible to separate the contributions of (perfect crystal) dynamic diffraction from those of (imperfect crystal) kinematic diffraction. The inability to perform this separation in a double crystal experiment is clear from fig. 3, where the small differences in kinematic scattering are superimposed on a much larger dynamical background. By eliminating the perfect crystal dynamical contributions from the experiment, even the relatively weak diffuse intensity can be observed.

One potential problem with the integration of the diffuse intensity in reciprocal space described above is that it neglects the fact that the incident X-ray beam has a slit-defined vertical divergence which is much larger than its perfect crystal collimated horizontal divergence. The effect of this vertical divergence will be to integrate the diffracted intensity in a direction perpendicular

Table 1

Relative excess integrated intensity measurements from the annealed LT-GaAs; the integrated intensities are given in arbitrary units and normalized to the control GaAs sample

Sample	Weighted integrated intensity (eq. (2))	Unweighted integrated intensity (eq. (3))
Perfect Ge	0	0
GaAs, control	1.0	1.0
LT-GaAs, 700°C	1.4	1.4
LT-GaAs, 800°C	2.5	2.3
LT-GaAs, 900°C	4.9	3.7

to the plane that is defined by the incident and diffracted wavevectors  $S_0/\lambda$  and  $S/\lambda$ . If the vertical divergence integrates all of the diffracted intensity, then the total excess intensity can be determined from a simple area integration in reciprocal space:

$$I_{\text{excess}} = 2 \int_{-q_y}^{+q_y} \int_{q_{x,\text{min}}}^{q_{x,\text{max}}} I_{\text{net}}(q_x, q_y) dq_x dq_y. \quad (3)$$

One can then proceed to calculate the excess intensity from the LT-GaAs as a function of annealing conditions using either eq. (2) ( $q_x$  weighted volume integration) or eq. (3) (unweighted area integration). The results of these calculations are shown in table 1 for the samples examined in this study. The integrated intensities in the table are given in arbitrary units, normalized to the integrated diffuse intensity from the control sample with a conventional GaAs epitaxial layer grown at 600°C. The values of  $I_{\text{excess}}$  were calculated using  $q_{x,\text{min}}$ 's chosen so that the excluded volume in reciprocal space corresponded to a cylinder of diameter of  $1 \times 10^{-4} \text{ \AA}^{-1}$ . This particular choice caused the excess intensity from the highly perfect Ge scan to equal zero. The same excluded volume was used for all samples.

The data in table 1 show that the kinematic scattering from the annealed LT-GaAs is greater than that from the control sample for all anneal conditions, irregardless of the integration method that is used. Furthermore, an increase in the anneal temperature from 700 to 900°C caused the

diffuse scattered intensity to increase by approximately a factor of three. This increase in the magnitude of diffuse scattering with increasing anneal temperature is in contrast with similar analyses of annealed bulk GaAs, where no increase in diffuse scattering was observed following anneals up to 900°C [26]. We therefore attribute the increase in excess scattering to an increase in the magnitude of diffuse scattering caused by the formation of arsenic precipitates in the LT-GaAs. Since the kinematic scattering is isotropic and is located in the vicinity of the GaAs 004 RLP, we believe that this scattering arises from strains in the host GaAs lattice caused by the growth of As-rich or arsenic precipitates. Of course, similar behavior is well known in the case of oxygen precipitation in silicon, where distortions in the Si lattice caused by the growth of  $\text{SiO}_2$  precipitates result in a large increase in the diffracted intensity measured (for instance) in a Lang topography experiment [14,25]. We thus conclude that the process of arsenic precipitation in LT-GaAs is reminiscent of oxygen precipitation in Czochralski silicon, despite the fact that oxygen precipitation requires a supersaturation of approximately 30 parts per million while the comparable process in GaAs occurs with arsenic concentrations of about 1%. It is interesting to speculate how the extensive literature on oxygen precipitation in silicon might be applicable to arsenic precipitation in GaAs. In addition to the formation of dislocation loops during precipitate growth, one could speculate about the formation of denuded zones in GaAs and intrinsic gettering of impurities. Clearly more work is needed to determine if the desirable characteristics of LT-GaAs could be improved still further by appeal to "wafer engineering" approaches that are well known in silicon processing.

## 5. Conclusions

In conclusion, we have used high resolution X-ray diffraction techniques to characterize the structural properties of GaAs grown at low temperature by MBE and to understand the effect of arsenic precipitates on the lattice of the epitaxial

layer. Both double crystal and triple crystal diffraction analyses have demonstrated that the crystallographic quality of the material examined in this study is extremely high, as evidenced by the presence of well defined interference fringes in the as-grown material and the absence of diffuse scattering around the layer's 004 RLP. Triple crystal X-ray diffraction demonstrated an increase in the apparent mosaic spread of the LT-GaAs with increasing anneal temperature; this increase has been put on a quantitative basis by defining it in terms of an "excess intensity" in reciprocal space. We attribute this observation to the presence of strain fields and distortions in the host GaAs in the epitaxial layer that arise when the thermally-induced arsenic precipitates nucleate and grow.

### Acknowledgements

The authors are grateful to S.L. Daniel for experimental assistance. They also wish to acknowledge Professor C.R. Wie for making his prior X-ray analyses of LT-GaAs available to the authors. The work at the University of Wisconsin was supported in part by the National Science Foundation through grants DMR-8907372 and ECS-9009595, while the work at Purdue University was partially supported by the Office of Naval Research under grant N00014-89-J-1864.

### References

- [1] F.W. Smith, A.R. Calawa, C.L. Chen, M.J. Mantra and L.J. Mahoney, IEEE Electron Device Letters EDL-9 (1988) 77.
- [2] M.R. Melloch, D.C. Miller and B. Das, Appl. Phys. Letters 54 (1989) 943.
- [3] See G.L. Witt, R. Calawa, U. Mishra and E. Weber, Eds., Low Temperature (LT) GaAs and Related Materials, Mater. Res. Soc. Symp. Proc., Vol. 241 (Materials Research Society, Pittsburgh, PA, 1992).
- [4] M. Kaminska, Z. Liliental-Weber, E.R. Weber, T. George, J.B. Kortright, F.W. Smith, B.-Y. Tsaur and A.R. Calawa, Appl. Phys. Letters 54 (1989) 1881.
- [5] M. Kaminska, E.R. Weber, Z. Liliental-Weber, R. Leon and Z.U. Rek, J. Vacuum Sci. Technol. B 7 (1989) 710.
- [6] Z. Liliental-Weber, W. Swider, K.M. Yu, J.B. Kortright, F.W. Smith and A.R. Calawa, Appl. Phys. Letters 58 (1991) 2153.
- [7] Z. Liliental-Weber, G. Cooper, R. Mariella and C. Kocot, J. Vacuum Sci. Technol. B 9 (1991) 2323.
- [8] K. Mahalingam, N. Otsuka, M.R. Melloch, J.M. Woodall and A.C. Warren, J. Vacuum Sci. Technol. B 9 (1991) 2328.
- [9] M.R. Melloch, N. Otsuka, K. Mahalingam, A.C. Warren, J.M. Woodall and P.D. Kirchner, in ref. [3], p. 113.
- [10] Z. Liliental-Weber, A. Clavierie, J. Washburn, F. Smith and R. Calawa, Appl. Phys. A 53 (1991) 141.
- [11] M. Fatemi, B. Tadayon, H.B. Dietrich and S. Tadayon, in ref. [3], p. 137.
- [12] C.R. Wie, K. Xie, D.C. Look, K.R. Evans and C.E. Stutz, in: Proc. 6th Conf. on Semi-Insulating III-V Materials, Toronto, 1990, Eds. A. Milnes and J.C. Miner (Institute of Physics, Bristol, 1990) p. 71.
- [13] C.R. Wie, K. Xie, T.T. Bardin, J.G. Pronko, D.C. Look, K.R. Evans and C.E. Stutz, Mater. Res. Soc. Symp. Proc. 198 (1990) 383.
- [14] H.R. Huff, H.F. Schaake, J.T. Robinson, S.C. Baber and D. Wong, J. Electrochem. Soc. 130 (1983) 1521.
- [15] P.F. Fewster, J. Appl. Cryst. 24 (1991) 178.
- [16] R.J. Matyi, M.R. Melloch and J.M. Woodall, Appl. Phys. Letters 60 (1992) 2642.
- [17] R.J. Matyi, Rev. Sci. Instr. 63 (1992) 5591.
- [18] Rocking-Curve Analysis by Dynamical Simulation (RADS) software, version 1.2 (available from Bede Scientific Instruments, Ltd., Durham, UK).
- [19] M.A. Hart and A.R.D. Rodrigues, Phil. Mag. 40 (1979) 149.
- [20] B.K. Tanner and M.A.G. Halliwell, Semicond. Sci. Technol. 3 (1988) 967.
- [21] J.R. Patel, J. Appl. Phys. 44 (1973) 3903.
- [22] A. Iida and K. Kohra, Phys. Status Solidi (a) 51 (1979) 533.
- [23] S.R. Andrews and S.R. Cowley, J. Phys. C (Solid State Phys.) 18 (1985) 6427.
- [24] V.S. Wang and R.J. Matyi, J. Appl. Phys. 72 (1993) 5158.
- [25] T.J. Shaffner, R.J. Matyi, A.E. Stephens and F.O. Meyer, X-ray topographic characterization of oxygen in lightly and heavily doped Czochralski silicon Electrochemical Society Extended Abstracts 85-2 (Electrochemical Society, Pennington, NJ, 1985) p. 482
- [26] R.J. Matyi, in preparation.